W-Band ENDOR Investigation of the Manganese-Binding Site of Concanavalin A: Determination of Proton Hyperfine Couplings and Their Signs

Palanichamy Manikandan,[†] Raanan Carmieli,[†] Tania Shane,[†] A. Joseph Kalb (Gilboa),[‡] and Daniella Goldfarb*,[†]

Contribution from the Departments of Chemical Physics and Structural Biology, Weizmann Institute of Science, Rehovot-76100, Israel

Received September 20, 1999. Revised Manuscript Received January 3, 2000

Abstract: W-band (95 GHz) pulsed EPR and electron−nuclear double resonance spectroscopic techniques were used to investigate the manganese S1 binding site of the protein concanavalin A in a frozen solution and in a single crystal. ^{1}H ENDOR spectra were collected by using the Davies ENDOR sequence, whereas Mims ENDOR was applied to record ^{2}H ENDOR spectra. Different EPR transitions were selected by performing the ENDOR measurements at different magnetic fields within the EPR spectrum. This selection, combined with the large thermal polarization achieved at magnetic fields of ∼3.4 T at low temperatures, allowed the assignment of ENDOR signals to their respective M_S manifolds, thus providing the sign of the hyperfine couplings. The exchangeable and nonexchangeable protons were differentiated by comparing ^{1}H and ^{2}H ENDOR spectra of a solution of the protein prepared in D_2O and of crystals soaked in D_2O. The two imidazole protons, located on the carbons flanking the Mn-bound nitrogen, are magnetically equivalent, situated 3.56 Å from the Mn^{2+} and their hyperfine coupling is purely dipolar. The four protons of the two water ligands are all inequivalent, and four values of $A_{||}$ and $A_{\perp}$ were determined. All possible combinations of these values yield distances in the range of 2.67 to 3.24 Å and a_{iso} between −1.13 and 1.37 MHz. By limiting a_{iso} to positive values, only four distances remain, 2.67, 2.76, 2.99, and 3.24 Å, corresponding to the four $Mn-H_{water}$ distances.

Introduction

Recent advances in high-field electron paramagnetic resonance (EPR) and electron−nuclear double resonance (ENDOR) spectroscopies offer new opportunities for the investigation of paramagnetic metal ion sites of metalloproteins in frozen solutions and single crystals.[1−8] This is particularly important for high-spin centers such as Mn^{2+} ($S = {}^5/_2$, $I = {}^5/_2$) due to considerable improvements in the resolution of the central EPR transitions ($|-{}^1/_2,m\rangle \rightarrow |{}^1/_2,m\rangle$) as a consequence of the reduced intensities of the forbidden transitions, ($|-{}^1/_2,m\rangle \rightarrow |{}^1/_2,m \pm 1\rangle$).[9,10] The weaker orientation dependence of the central EPR transition at high fields reduces inhomogeneous broadening in orientationally disordered samples leading to further improvements in resolution.[9,11] The line narrowing also enhances the sensitivity in the corresponding ENDOR experiments.[12] In addition, the large energy gap between the different EPR transitions in the case of a dominant electron Zeeman interaction leads to a large thermal polarization at low temperatures, thus allowing straightforward determination of the sign of the hyperfine coupling.[13] Finally, the large absolute sensitivity facilitates considerably measurements of size limited samples such as single crystals of protein.[4−6] In this work we describe pulsed W-band EPR and ENDOR measurements on a frozen solution and a single crystal of the Mn^{2+}-containing protein concanavalin A. We also present a strategy for signal assignment and determination of magnitude and sign of the principal components of the hyperfine interaction of various protons coupled to the Mn^{2+}.

Concanavalin A is a member of the plant haemagglutinin (or plant lectin) family; a large and ubiquitous group of saccharide-binding proteins whose biological function is as yet unknown.[14]

[†] Department of Chemical Physics.

[‡] Department of Structural Biology.

(1) Lebedev, Ya. S. In *Modern Pulsed and Continuous-wave Electron Spin Resonance*; Kevan, L., Bowman, M. K., Eds.; Wiley: New York, 1990; pp 365−436.

(2) Möbius, K. In *Biological Magnetic Resonance*; Berliner, L. J., Reuben, J., Eds.; Plenum Press: New York, 1993; Vol. 13, pp 253−274.

(3) Burghaus, O.; Rohrer, M.; Gotzinger, T.; Plato, M.; Möbius, K. *Meas. Sci. Technol.* **1992**, *3*, 765.

(4) Coremans, J. W. A.; Poluektov, O. G.; Groenen, E. J. J.; Canters, G. W.; Nar, H.; Messerschmidt, A. *J. Am. Chem. Soc.* **1994**, *116*, 3037.

(5) Coremans, J. W. A.; van Gastel, M.; Poluektov, O. G.; Groenen, E. J. J.; den Blaauwen, T.; van Pouderoyen, G.; Canters, G. W.; Nar, H.; Hammann, C.; Messerschmidt, A. *Chem. Phys. Lett.* **1995**, *235*, 202.

(6) Coremans, J. W. A.; Poluektov, O. G.; Groenen, E. J. J.; Canters, G. W.; Nar, H.; Messerschmidt, A. *J. Am. Chem. Soc.* **1996**, *118*, 12141.

(7) Earle, K. A.; Budil, D. E.; Freed, J. H. In *Advances in Magnatic and Optical Resonances*; Warren, W. S., Ed.; Academic Press: New York, 1996; Vol. 19, pp 253−323.

(8) Prisner, T. F. In *Advances in Magnetic and Optical Resonances*; Warren, W. S., Ed.; Academic Press: New York, 1997; Vol. 20, pp 245−299.

(9) Abragam, A.; Bleaney, B. *Electron Paramagnetic Resonance of Transition Ions*; Clarendon Press: Oxford, 1970.

(10) Meirovitch, E.; Luz, Z.; Kalb, A. J. *J. Am. Chem. Soc.* **1974**, *96*, 7538.

(11) Reed, G. H.; Markham, G. D. In *Biological Magnetic Resonance*; Berliner, L. J., Reuben, J., Eds.; Plenum Press: New York, 1984; Vol. 6, p 73.

(12) Arieli, D.; Vaughan, D. E. W.; Strohmaier, K. G.; Goldfarb, D. *J. Am. Chem. Soc.* **1999**, *121*, 6028.

(13) Goldfarb, D.; Strohmaier, K. G.; Vaughan, D. E. W.; Thomann, H.; Poluektov, O. G.; Schmidt, J. *J. Am. Chem. Soc.* **1996**, *118*, 4665.

(14) Kalb (Gilboa), A. J.; Habash, J.; Hunter, N. S.; Price, H. J.; Raftery, J.; Helliwell, J. R. In *Metal Ions in Biological Systems*; Sigel, A., Sigel, H., Eds.; M. Dekker: New York, 2000; Vol. 37, pp 279−300.

10.1021/ja993395z CCC: $19.00
Published on Web 03/25/2000

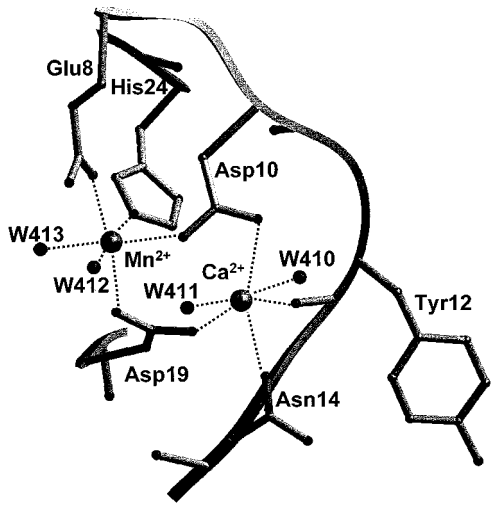

Figure 1. The structure of the Mn^{2+} and Ca^{2+} sites of concanavalin A.[19]

The importance of these proteins is expressed in their ability to bind saccharides; each member of the family has a unique saccharide specificity. Concanavalin A was the first plant haemagglutinin to be characterized crystallographically[15] and its crystal structure was solved in 1972 at 2.0 Å resolution.[16,17] The protein has two metal ion binding sites which are essential for saccharide binding. The first site, referred to as the transition-metal-binding site, S1, can accommodate Mn^{2+}, Co^{2+}, Ni^{2+}, Zn^{2+}, or Cd^{2+} ions, whereas the second site, S2, termed the calcium-binding site, binds Ca^{2+} or Cd^{2+} ions.[18] Recently, the structure of concanavalin A, with Mn^{2+} and Ca^{2+} ions in S1 and S2, respectively, has been determined at ultrahigh resolution (0.94 Å) with exceptional accuracy and precision.[19] In the crystal (space group $I222$, $a = 89.6$, $b = 86.5$, $c = 62.1$ Å) the concanavalin A monomer associates as a dimer of dimers to form a tetramer of approximately 100 KDa. The transition-metal-binding site is characterized by a slightly distorted octahedral symmetry involving the ligation of the central metal ion to three carboxyl oxygens, one nitrogen from a histidine residue, and two water oxygens, as shown in Figure 1.[19]

Concanavalin A has been studied in the past by EPR spectroscopy. The zero-field splitting (ZFS) tensor of the Mn^{2+} ion was determined by single-crystal Q-band continuous wave (CW) EPR spectroscopy.[10] The ligand environment of concanavalin A was investigated by three-pulse electron-spin echo envelope modulation (ESEEM) experiments on a lyophilized powder and the frequencies observed were assigned to one of the ^{14}N nuclei of His24.[20] Later, additional ESEEM experiments, carried out on a frozen solution of concanavalin A, assigned the modulations specifically to the directly bound nitrogen, rather than to the remote one.[21] A lyophilized powder of concanavalin A was also used to demonstrate that it is possible to observe ^{55}Mn signals in X-band pulsed ENDOR experiments.[22] The present study is the first investigation of the hyperfine coupling of protons in the Mn site.

The high-resolution structure of concanavalin A makes it an excellent candidate for quantitative determination of the relation between the magnetic tensors of the coupled nuclei in the Mn^{2+} site and the atomic coordinates. This can then be used as a reference for Mn^{2+} sites in systems with unknown structures where Mn^{2+} is often coordinated to histidine residues or water molecules. This will not only serve for naturally occurring Mn^{2+} sites but also in many instances where a Mn^{2+} ion is used as a probe, substituted for other metal ions such as Mg^{2+}. In this manuscript we report the hyperfine principal components of the four protons of the two water ligands and the two protons of the imidazole moiety from detailed ENDOR studies of frozen solutions of concanavalin A. While the four water protons are found to be magnetically inequivalent, the two nonexchangeable imidazole protons are magnetically equivalent. In addition we present preliminary ^1H ENDOR results from single crystals where the signal assignment was carried out applying the strategy developed for the frozen solutions.

Experimental Section

Sample Preparation and Crystal Growth. Concanavalin A containing 20 mol % Mn^{2+} was purchased from Sigma as a lyophilized powder. The crystallization buffer (XTAL) was prepared as reported earlier.[15] A 1.6 mM (in monomer) solution of concanavalin A in 40% glycerol in XTAL buffer was used for the frozen solution measurements. A similar solution was prepared in glycerol-d_3 and XTAL buffer in 99.9% D_2O for the assignment of exchangeable protons. Approximately 2 μL of each solution were placed in a 0.9-mm-o.d. quartz tube, which was carefully sealed. The deuterium-exchanged samples were handled in a dry Argon atmosphere to prevent exchange with atmospheric H_2O.

Single crystals of concanavalin A were grown as follows:[14,23] the concanavalin A powder was dissolved in a saturated NaCl solution, gently shaken at 313 K for 2 h, centrifuged briefly at room temperature to remove a small amount of insoluble material, and passed through a Millipore filter of 0.22 μm pore size. Dialysis bags containing small portions (0.2 mL) of the above solution were immersed in vials containing XTAL buffer and incubated at 303 K for several days, until sizable crystals of regular morphology appeared in the dialysis bags. The shape of the crystals obtained from the crystallization protein solution depends on the experimental procedures and conditions used. The EPR/ENDOR studies require crystals with a moderate size and a well-defined morphology. The current crystallization procedure[14] produces well-shaped crystals with one of the edges parallel to the crystallographic *b*-axis and the other two axes perpendicular to it. Crystals of appropriate size were chosen and transferred into a XTAL/MPD (2-methyl-2,4-pentanediol) (50:50%) solution, where MPD serves as a cryoprotectant. The crystals were mounted with the aid of a polarizing microscope into 0.9-mm-o.d. thin-walled quartz tubes with their crystallographic *b*-axis, corresponding to the longest dimension of the crystal, parallel to the long axis of the tube. The excess of liquid was carefully removed with the help of a filter paper, until the crystal was barely wet and the tube was flame sealed at both ends. The exact orientation of the crystal was determined by brief X-ray diffraction measurements. The approximate crystal size was $0.8 \times 0.4 \times 0.3$ mm.

Spectroscopic Measurements. Field-sweep (FS) echo-detected (ED) EPR and pulsed ENDOR spectra were recorded at 4.4−4.6 K on a home-built spectrometer operating at 94.9 GHz.[24] FS-ED EPR spectra were measured with the two-pulse echo sequence ($\pi/2-\tau-\pi-\tau-$echo) where the echo intensity is registered as a function of the magnetic field. Typically, microwave (MW) pulse lengths (t_{MW}) of 0.05 and 0.1 μs were used with $\tau = 0.25$ μs. The magnetic field values were calibrated by using the proton Larmor frequency, as determined by the ENDOR measurements. The ^1H ENDOR spectra were measured with the Davies ENDOR pulse sequence ($\pi-T-\pi/2-\tau-\pi-\tau-$echo

(15) Greer, J.; Kaufman, H. W.; Kalb, A. J. *J. Mol. Biol.* **1970**, *48*, 365.
(16) Edelman, G. M.; Cunningham, B. A.; Reeke, G. N.; Becker, J. W., Jr. *Proc. Natl. Acad. Sci., U.S.A.* **1972**, *69*, 2580.
(17) Hardman, K. D.; Ainsworth, C. F. *Biochemistry* **1972**, *11*, 4910.
(18) Shoham, M.; Kalb, A. J.; Pecht, I. *J. Biol. Chem.* **1973**, *248*, 549.
(19) Deacon, A.; Gleichmann, T.; Kalb (Gilboa), A. J.; Price, H.; Raftery, J.; Bradbrook, G.; Yariv, J.; Helliwell, R. *J. Chem. Soc., Faraday Trans.* **1997**, *93*, 4305.
(20) LoBrutto, R.; Smithers, G. W.; Reed, G. H.; Orme-Johnson, W. H.; Tan, S. L.; Leigh, J. S. *Biochemistry* **1986**, *25*, 5654.
(21) McCracken, J.; Peisach, J.; Bhattacharyya, L.; Brewer, F. *Biochemistry* **1991**, *30*, 4486.
(22) Sturgeon, B. E.; Ball, J. A.; Randall, D. W.; Britt, R. D. *J. Phys. Chem.* **1994**, *98*, 12871.
(23) Weinzierl, J.; Kalb, A. J. *FEBS Lett.* **1971**, *18*, 268.
(24) Gromov, I.; Krymov, V.; Manikandan, P.; Arieli, D.; Goldfarb, D. J. *Magn. Reson.* **1999**, *139*, 8.

with an RF pulse applied during the time interval T).[25] The Mims ENDOR sequence ($\pi/2-\tau-\pi/2-T-\pi/2-\tau-$echo with an RF pulse applied during the time T) was used in the ^{2}H ENDOR measurements.[26] The experimental conditions were $t_{MW} = 0.2$, 0.1, 0.2 μs, $\tau = 0.4$ μs, $t_{RF} = 25$ μs in the Davies ENDOR experiments, and $t_{MW} = 0.1$, 0.1, 0.1 μs, $\tau = 0.25$ μs, $t_{RF} = 40$ μs for the Mims ENDOR measurements. The intensity and frequency scales of the ^2H spectra were multiplied by -1 and γ^H/γ^D (= 6.5144), respectively, to allow a convenient comparison with the ^{1}H ENDOR spectra. The frequency scale in the ^{1}H and ^{2}H ENDOR spectra is given with respect to the Larmor frequency, $\nu = \nu_{RF} - \nu_I$. X-band FS-ED spectra were recorded at 4.2 K on a home-built spectrometer at 9.323 GHz described elsewhere.[27] In these measurements $t_{MW} = 0.02$, 0.04 μs and $\tau = 0.3$ μs.

Theory. A brief summary of the spectral characteristics of a $S = {}^5/_2$ system coupled to nuclei with $I = {}^1/_2$, $I = 1$, or $I = {}^5/_2$ is presented below. A schematic energy level diagram for a $S = {}^5/_2$, $I = {}^1/_2$ under the conditions of a dominant isotropic electron Zeeman interaction is shown in Figure 2. There are totally five allowed EPR transitions, the splittings of which depend on the ZFS parameters, D and E. While the central, $|-{}^1/_2,m\rangle \rightarrow |{}^1/_2,m\rangle$, EPR transitions frequencies are only weakly dependent on the orientation of the external magnetic field, $\vec{B}$, with respect to the principal axis system of the ZFS, all other EPR transitions are highly orientation dependent. Hence, the spectrum of an orientationally disordered system exhibits a narrow central lines at $g \sim 2$, due to the central transitions, superimposed on a broad background corresponding to all other EPR transitions.[9,28] There are six ENDOR transitions whose frequencies are given by[29,30]

$$\nu_{M_S}^{ENDOR} = [(M_S A - \nu_I)^2 - M_S{}^2 B^2]^{1/2} \quad (1)$$

where ν_I is the nuclear Larmor frequency, $A = T_\perp(3\cos^2\theta - 1) + a_{iso}$, $B = 3T_\perp \sin\theta\cos\theta$, and θ is the angle between the direction of the unique axis of the hyperfine interaction and $\vec{B}$ and a_{iso} is the isotropic hyperfine constant. In eq 1 the hyperfine interaction is assumed to be axially symmetric. When the point-dipole approximation applies, $T_\perp = (g g_n \beta\beta_n)/(hr^3)$ where r is the internuclear distance and the unique axis is along $\vec{r}$. At the canonical orientations, the hyperfine splittings are $A_{||}(M_S) = M_S(2T_\perp + a_{iso})$ and $A_\perp(M_S) = M_S(a_{iso} - T_\perp)$.

The frequency separation of the various EPR transitions is significantly larger than the MW pulse bandwidth even for a sample with a small D value. Therefore, only one EPR transition is selected for each spin packet during a pulse experiment. However, due to the inhomogeneous nature of the EPR spectrum, the selection of a particular magnetic field results in the excitation of a number of overlapping EPR transitions arising from different spin packets (molecules). Figure 2 presents the schematic ENDOR spectrum obtained for each EPR transition. Only that corresponding to a $|-{}^1/_2,m\rangle \rightarrow |{}^1/_2,m\rangle$ EPR transition appears symmetric about the nuclear Larmor frequency. At $\sim$3.3 T ($g \simeq 2$) and low temperatures, the EPR transitions become highly thermally polarized (see Table 1) and the contributions of the $|{}^1/_2,m\rangle \rightarrow |{}^3/_2,m\rangle$ and $|{}^3/_2,m\rangle \rightarrow |{}^5/_2,m\rangle$ EPR transitions to the ENDOR spectrum become very small. In principle, the ENDOR spectrum should exhibit strong signals from the $M_S = -{}^5/_2$, $-{}^3/_2$ manifolds but due to their larger anisotropies in orientationally disordered samples they are significantly broader than those of the $M_S = \pm{}^1/_2$ manifolds and are therefore harder to detect.

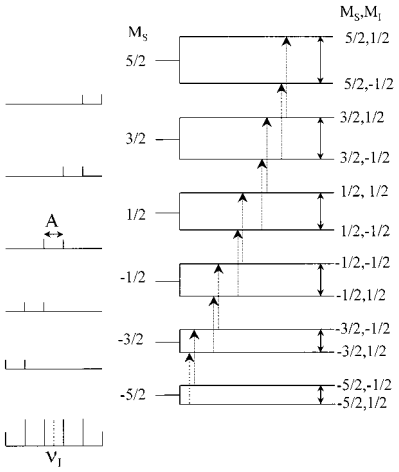

Figure 2. Schematic energy level diagram for a $S = {}^5/_2$, $I = {}^1/_2$ spin system with a dominating electron Zeeman interaction and the ENDOR spectra for each EPR transition for weak coupling ($2\nu_I > A$). The dotted arrows represent allowed EPR transitions and the other arrows label ENDOR transitions.

Table 1. Calculated Relative Populations for the Different Electronic Spin Manifolds of Mn^{2+} at 94.9 GHz and 4.4 K

energy level	$-{}^5/_2$	$-{}^3/_2$	$-{}^1/_2$	${}^1/_2$	${}^3/_2$	${}^5/_2$
relative population	1.0	0.35	0.12	0.04	0.015	0.005

When $I = 1$, there are two ENDOR transitions for each M_S manifold, given to first order by[31,32]

$$\nu_{M_S}^{ENDOR}(\pm) = \nu_{M_S}^{ENDOR} \pm 3P/2 \quad (2)$$

where P is the angle-dependent quadrupole-splitting.

In the case of Mn^{2+} there is an additional splitting due to the ^{55}Mn hyperfine interaction. This interaction does not affect the ENDOR frequencies of ^{1}H or ^{2}H coupled nuclei. The structure of the ENDOR spectrum of ^{55}Mn has been described in detail by Sturgeon et al.[22] For each EPR transition the ENDOR spectrum consists of a doublet centered at $\overline{\Delta\nu}$ with a splitting of $\Delta\nu$, given by the first-order perturbation corrected expressions:

$$\Delta\nu = 2\nu_I + \frac{a_{iso}^2}{\nu_0}(S(S+1) - M_S^2)$$

$$\overline{\Delta\nu} = |a_{iso}M_S| - \frac{a_{iso}|a_{iso}M_S|}{2\nu_0}(2m_I \pm 1) \quad (3)$$

where ν_0 is the spectrometer frequency.

Results

Frozen Solutions. The FS-ED EPR spectrum of a frozen solution of concanavalin A is shown in the inset of Figure 3. It consists of a well-resolved sextet superimposed on a broad asymmetric background with a total width of about 1000 G. The six narrow peaks correspond to the ^{55}Mn ($I = {}^5/_2$) hyperfine components of the $|-{}^1/_2,m> \rightarrow |{}^1/_2,m\rangle$ EPR transitions centered at $g = 2$. The background is due to a superposition of the powder patterns of all other EPR transitions with intensities in the following order: $|-{}^5/_2,m\rangle \rightarrow |-{}^3/_2,m\rangle > |-{}^3/_2,m\rangle \rightarrow |-{}^1/_2,m\rangle > |{}^1/_2,m\rangle \rightarrow |{}^3/_2,m\rangle > |{}^3/_2,m\rangle \rightarrow |{}^5/_2,m\rangle$ due to the Boltzmann distribution (see Table 1). The frequencies of these transitions exhibit a first-order dependence on the ZFS, resulting in powder patterns in orientationally disordered systems where the hyperfine structure is unresolved. In contrast, the $|-{}^1/_2,m\rangle \rightarrow |{}^1/_2,m\rangle$ transition frequencies are affected by the ZFS only to second

(25) Davies, E. R. *Phys. Lett.* **1974**, *47A*, 1.
(26) Mims, W. B. *Proc. R. Soc. London, Ser. A* **1965**, *283*, 452.
(27) Shane, J. J.; Gromov, I.; Vega, S.; Goldfarb, D. *Rev. Sci. Instrum.* **1998**, *69*, 3357.
(28) Gaffney, B. J.; Silverstone, H. J. In *Biological Magnetic Resonance*; Berliner, L. J., Reuben, J., Eds.; Plenum Press: New York, 1993; Vol. 13, pp 1−57.
(29) Tan, X.; Bernardo, M.; Thomann, H.; Scholes, C. P. *J. Chem. Phys.* **1993**, *98*, 5147.
(30) Kurreck, H.; Kirste, B.; Lubitz, W. Electron Nuclear Double Resonance Spectroscopy of Radicals in Solution Application to Organic and Biological Chemistry. VCH Publishers: New York, 1988.
(31) Hoffmann, B. M.; DeRose, V. J.; Doan, P. E.; Gurbiel, R. J.; Houseman, A. L. P.; Telser, J. In *Biological Magnetic Resonance*; Berliner, L. J., Reuben, J., Eds.; Plenum Press: New York, 1993; Vol. 13, pp 151−218.
(32) Gemperle, C.; Schweiger, A. *Chem. Rev.* **1991**, *91*, 1481.

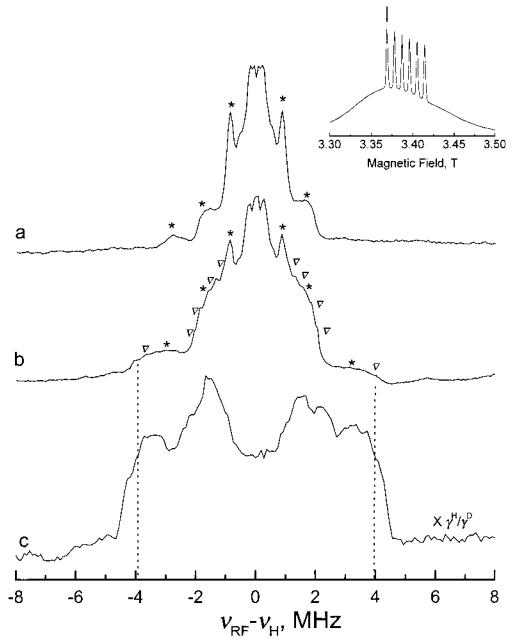

Figure 3. ^{1}H Davies ENDOR spectra (measured at 3.365 T) of 1.6 mM concanavalin A in (a) 40% glycerol-d_3 in XTAL(D_2O); (b) 40% glycerol in XTAL(H_2O); (c) ^{2}H Mims ENDOR spectra of the protein in 40% glycerol-d_3 in XTAL(D_2O). The inset shows the FS-ED EPR spectrum of the H_2O solution. The asterisks and triangles mark the H_{im} and H_w signals, respectively. The dotted lines mark the correspondence between the outer edges of the ^{1}H and ^{2}H ENDOR spectra (see text).

Table 2. Assignment of the ENDOR Lines of the Imidazole Protons, $H_{im1,2}$, to the Different M_S Manifolds

M_S	$\upsilon_\perp$ (±0.04), MHz	$\upsilon_\parallel$ (±0.05), MHz
$-3/2$	−2.8	5.25
$-1/2$	−0.86	1.77
$1/2$	0.86	−1.77
$3/2$	2.8	−5.25

order and therefore appear as intense sharp lines with resolved ^{55}Mn hyperfine splitting.[9,11]

The ^{1}H ENDOR spectrum, recorded at the low-field hyperfine component of the central EPR transition, marked by an arrow in the inset, is shown in Figure 3b. It consists of a number of superimposed powder patterns, symmetrically situated about the ^{1}H Larmor frequency, υ_H. The ENDOR signals of the nonexchangeable imidazole protons, H_{im1} and H_{im2}, were identified by exchanging the water protons with deuterium using a D_2O solution. The ^{1}H ENDOR spectrum of this solution, shown in Figure 3a, is considerably simpler than that of the H_2O solution (Figure 3b). It exhibits two powder patterns, the first, with $|A_\parallel| < 0.8$ MHz, is attributed to distant, weakly coupled protons and will no longer be discussed. The second, is axially symmetric with $|A_\parallel| = 3.54(\pm0.1)$ MHz and $|A_\perp| = 1.72(\pm0.08)$ MHz, assigned to the magnetically equivalent H_{im1} and H_{im2} protons. A clear additional peak situated asymmetrically at −2.8 MHz appears as well and its assignment is discussed below (see Table 2).

The ^{2}H ENDOR spectrum of the D_2O solution is shown in Figure 3c. The only exchangeable deuterons with a significant hyperfine coupling that contribute to this spectrum are the water deuterons, ^2H_w. The ^{2}H($I = 1$) ENDOR spectrum is more complicated than the corresponding ^{1}H spectrum since each line splits into a doublet due to the nuclear quadrupole interaction (see eq 2). For ^{2}H in an OD bond the maximum quadrupolar splitting is ∼0.3 MHz.[33,34] The ^{1}H and ^{2}H spectra can be conveniently compared by expanding the frequency scale of the ^{2}H spectrum by the factor γ^H/γ^D. When the hyperfine coupling is significantly larger than the quadrupole interaction a good correspondence in line positions is expected, except for small symmetrical shifts due to the quadrupole interaction which at this scale amounts to a maximum of ∼1.0 MHz. Accordingly, the powder pattern in Figure 3c corresponds rather well to the outer wings of the ^{1}H spectrum shown in Figure 3b as outlined by the guiding lines. The outmost shoulders in the ^{2}H spectrum are outside the range of the ^{1}H spectrum and are attributed to quadrupolar splittings. Comparison of the spectra shown in Figure 3 lead to the identification of the signals of the imidazole protons and water protons, marked by asterisks and triangles, respectively, in Figure 3a,b. This shows that the water protons, unlike the imidazole protons, are magnetically inequivalent. The specific assignment of the water singularities (marked by the triangles) requires field-dependent measurements as described below. While the large number of features corresponding to the water protons show that their hyperfine interactions are different, the low resolution of the ^{2}H spectrum does not allow one to draw any conclusions concerning their quadrupolar couplings.

The symmetric appearance of the spectra shown in Figure 3 indicates that they originate primarily from a $|-1/2,m\rangle \rightarrow |1/2,m\rangle$ EPR transition. However, considering the FS-ED spectrum and the field at which the spectra were measured, contributions from the $|-5/2,m\rangle \rightarrow |-3/2,m\rangle$ and $|-3/2,m\rangle \rightarrow |-1/2,m\rangle$ EPR transitions are expected as well. A close look at the low-frequency end of the spectra shown in Figure 3 indeed reveals signals from the $M_S = -3/2$ manifold. This is particularly evident in Figure 3a where a peak at −2.8 MHz appears while there is practically no intensity at 2.8 MHz. The signals of the $M_S = -3/2$ manifold seem significantly weaker than those of the $M_S = \pm1/2$ manifolds due to their larger anisotropy (see eq 1). The $M_S = -3/2$ signals become more prominent when the ENDOR spectrum is recorded at field positions where the central EPR transitions are not excited. Such experiments enable the assignment of the ENDOR signals to the various M_S manifolds.[29,35]

Figure 4 shows the ^{1}H ENDOR spectra of concanavalin A in the D_2O solution recorded at three resonant fields, marked with a, b, and c in the inset of the figure. The spectra measured at fields a and c are highly asymmetric and through comparison with the spectrum recorded at position b the canonical singularities of the $M_S = -1/2$ powder pattern of $H_{im1,2}$, originating from the $|-3/2,m\rangle \rightarrow |-1/2,m\rangle$ EPR transition, were identified at $\upsilon_\perp = -0.86(\pm0.04)$ and $\upsilon_\parallel = 1.77(\pm0.05)$ MHz. Using eq 1 with the frequencies of the various singularities in the asymmetric spectra and taking into account the relative intensities of the $\upsilon_\perp$ and $\upsilon_\parallel$ singularities in powder patterns arising from isotropic distributions, all spectral features were assigned as marked on Figure 4 and listed in Table 2. This yields $A_\perp = -1.72(\pm0.08)$ MHz, $A_\parallel = 3.54(\pm0.1)$ MHz, $a_{iso} = 0.0(\pm0.08)$, and $T_\perp = 1.75(\pm0.1)$ MHz. While the spectrum recorded at position a is mainly from the $|-3/2,m\rangle \rightarrow |-1/2,m\rangle$ EPR transitions, the spectrum measured at position c also shows ENDOR signals from $M_S = 1/2$ and $3/2$ manifolds. The relative intensities of these signals, compared to those of the $M_S = -1/2$ and $-3/2$ manifolds, are higher than expected by the mere population differences (see Table 1). This apparent discrepancy

(33) Weissmann, M. *J. Phys. Chem.* **1966**, *44*, 422.
(34) Spiess, H. W.; Garrett, B. B.; Sheline, R. K. *J. Phys. Chem.* **1969**, *51*, 1201.
(35) Vardi, R.; Bernardo, M.; Thomann, H.; Strohmaier, K. G.; Vaughan, D. E. W.; Goldfarb, D. *J. Magn. Reson.* **1997**, *126*, 229−241.

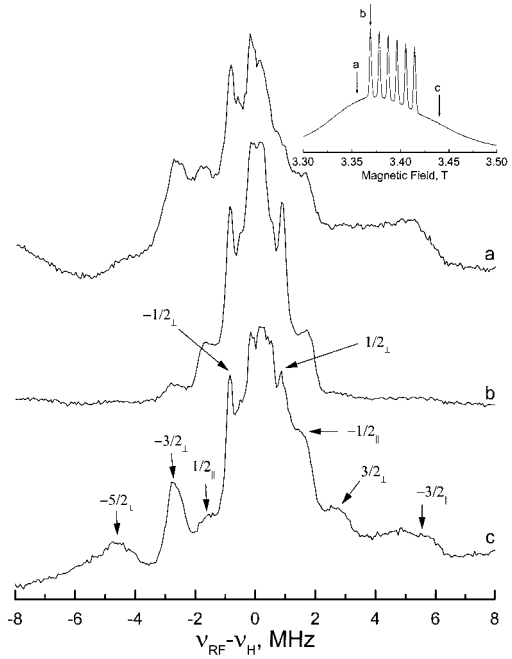

Figure 4. ^{1}H Davies ENDOR spectra of a frozen solution of 1.6 mM concanavalin A in 40% glycerol-d_3 in XTAL(D_2O) measured at (a) 3.342, (b) 3.365, and (c) 3.434 T. The inset shows the FS-ED EPR spectrum.

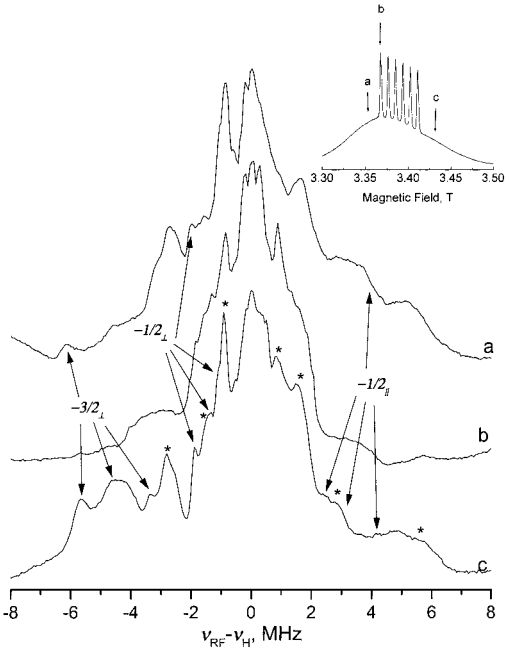

Figure 5. ^{1}H Davies ENDOR spectra of a frozen solution of 1.6 mM concanavalin A in 40% glycerol in XTAL(H_2O) measured at (a) 3.352, (b) 3.366, and (c) 3.428 T. The inset shows the FS-ED EPR spectrum.

is due to the powder line shape of the corresponding EPR transitions. If position c is close to the perpendicular singularity of the $|^1/_2,m\rangle \rightarrow |^3/_2,m\rangle$ powder patterns and the parallel singularity of the $|-^3/_2,m\rangle \rightarrow |-^1/_2,m\rangle$ patterns, then the relative intensity of the former will be enhanced compared to the Boltzmann distribution. In contrast, if position a is close to the perpendicular singularity of the $|-^3/_2,m\rangle \rightarrow |-^1/_2,m\rangle$ patterns and the parallel singularity of the $|^1/_2,m\rangle \rightarrow |^3/_2,m\rangle$ patterns, a very weak contribution of the latter to the ENDOR spectrum is expected. These differences in the relative intensities of the $M_S = -^3/_2$ and $^3/_2$ ENDOR signals measured at positions a and c provide indirectly the EPR line shape of the various EPR transitions indicating that the sign of D is positive.

The ^{1}H ENDOR spectra of a frozen solution of concanavalin A in H_2O recorded at three different fields are shown in Figure 5. The signals corresponding to $H_{im1,2}$ are marked by asterisks. The water ENDOR signals, identified by using the approach described above, show that the four water protons have four distinct hyperfine couplings. The ENDOR frequencies of the various M_S manifolds at the canonical orientations are indicated in Figure 5c and listed in Table 3.

Single Crystals. A single crystal of concanavalin A with a regular morphology was oriented with its *b*-axis parallel to the tube axis and the static magnetic field lying in the crystallographic *ac* plane. W-band FS-ED EPR spectra recorded for several orientations of the crystal relative to $\vec{B}$ are shown in Figure 6. The spectra exhibit two well-resolved sets of sharp sextets of the $|-^1/_2,m\rangle \rightarrow |^1/_2,m\rangle$ EPR transitions, corresponding to two spectroscopically distinct sites of the Mn^{2+} in this plane. The centers of the sextets vary with orientation and when the magnetic field direction is along the *c*-axis, the two sextets coincide.[10] At this orientation, the weak forbidden transitions, ($\Delta_{M_S} = \pm 1$, Δm_I (^{55}Mn) $= \pm 1$) situated between the sextet lines, become evident. The signals corresponding to the "other" EPR transitions are very broad and their ^{55}Mn hyperfine splitting is not resolved, although it exhibits some angular dependence. The low resolution of these transitions has been attributed to a mosaic spread of ZFS parameters.[10]

Table 3. Assignment of the ENDOR Lines of the Water Protons, H_w to the Different M_S Manifolds

M_S	$\upsilon_\perp$ (±0.04), MHz				$\upsilon_\parallel$ (±0.05), MHz			
$-^3/_2$	−3.3,	−4.56,	−5.68,	−6.25	not detected			
$-^1/_2$	−1.06,	−1.44,	−1.86,	−2.06	3.00,	4.17,	2.43,	3.77
$^1/_2$	1.06,	1.44,	1.86,	2.06	−3.00,	−4.17,	−2.43,	−3.77

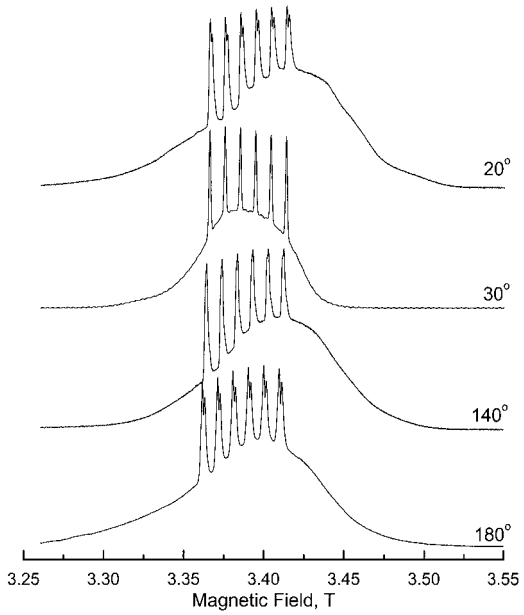

Figure 6. W-band FS-ED EPR spectra of a single crystal of concanavalin A with the magnetic field in the *ac* plane. The angles correspond to an arbitrary 0° position.

The high resolution of the central transitions allows straightforward identification of the spectroscopically distinct sites of Mn^{2+}. This facilitates significantly the collection of ENDOR rotation patterns where the EPR signal of a particular site has to be tracked. For comparison we present in Figure 7 a series

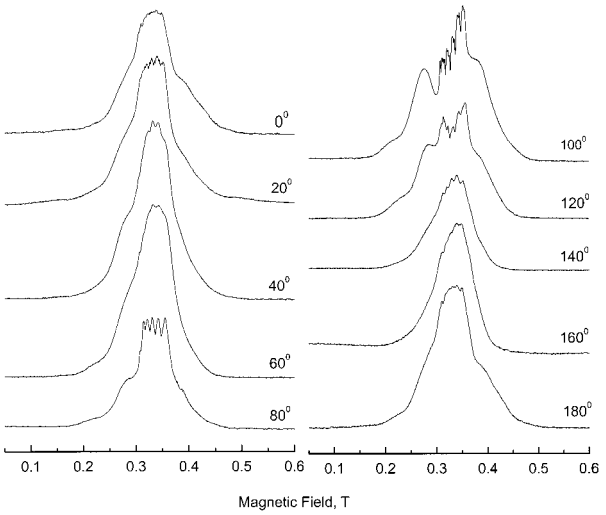

Figure 7. X-band FS-ED EPR spectra (4.2 K) of a single crystal of concanavalin A with the magnetic field in an arbitrary plane.

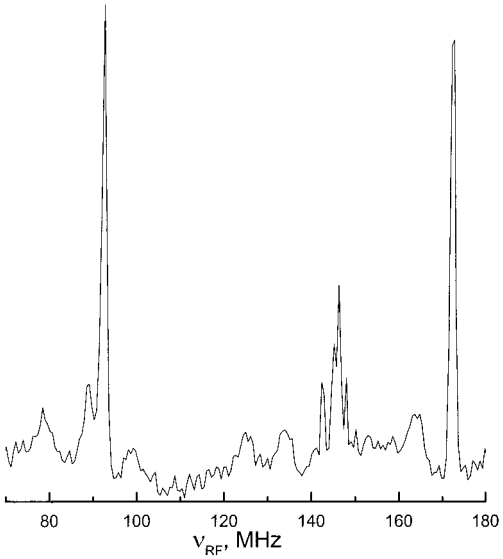

Figure 8. ^{55}Mn Davies ENDOR spectrum of a single crystal of concanavalin A oriented with the magnetic field along the crystallographic *c*-axis. Experimental conditions: $t_{MW} = 0.07, 0.035, 0.07$ μs, $\tau = 0.35$ μs, $t_{RF} = 6$ μs, $B_0 = 3.413$ T.

of FS-ED EPR spectra recorded at X-band for an arbitrary crystallographic plane. The crystal used for the X-band measurements had to be larger than those used for the W-band measurements and it had an ill-defined morphology, which made its alignment and the identification of the crystallographic axes difficult. The sextet of the central transition is not well resolved in many orientations and the different Mn^{2+} sites cannot be identified, thus making the collection of ENDOR rotation patterns rather difficult in terms of the choice of the resonant magnetic field. In contrast, the four Mn^{2+} sites in a crystal oriented in an arbitrary plane are well resolved at W-band (not shown).

The crystal was rotated around its *b*-axis until the magnetic field was collinear with the crystallographic *c*-axis and all four symmetry related Mn(II) sites in the tetramer are magnetically equivalent (see Figure 6, the 30° trace). From the sextet splitting a_{iso} (^{55}Mn) = 266 MHz was obtained. The ^{55}Mn ENDOR spectrum recorded at this orientation and the field set to the highest field hyperfine component is shown in Figure 8. It shows a doublet, arising from the $M_S = \pm^1/_2$ manifolds, centered at $\overline{\Delta\nu} = 132.4$ MHz with a splitting, $\Delta\nu$, of 79.8 MHz. The

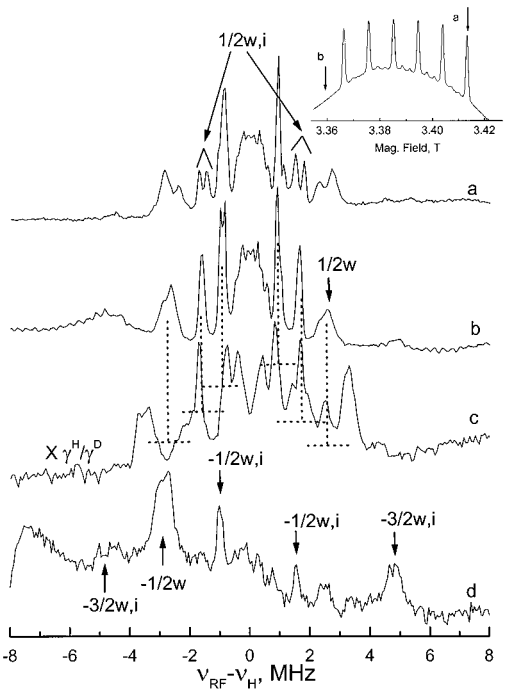

Figure 9. ENDOR spectra of a single crystal of concanavalin A oriented with the magnetic field along the crystallographic *c*-axis. (a) ^{1}H Davies ENDOR of concanavalin A(H_2O), recorded at a resonant magnetic field indicated by a in the inset ($B_0 = 3.4124$ T). (b) Similar to (a) for concanavalin A(D_2O). (c) ^{2}H Mims ENDOR of concanavalin A recorded position a. (d) ^{1}H Davies ENDOR of concanavalin A(D_2O), recorded at a resonant magnetic field indicated by b in the inset ($B_0 = 3.4126$ T). Signals marked with w and i indicate water and imidazole protons, respectively.

splitting of 79.8 MHz is larger than $2\nu_I$, which at this field should be 71.9 MHz. This deviation is due to higher order terms of the hyperfine coupling.[22] Using eq 3 and the a_{iso} value obtained from the FS-ED EPR spectrum we obtain for the doublet splitting $\Delta\nu = 78.0$ MHz and for its center, $\overline{\Delta\nu} = 129.8$ MHz, which is in good agreement with experimental results. The sharp lines near 145 MHz are due to protons and other broad peaks are due to baseline problems.

The ^{1}H ENDOR spectrum recorded with the field along the *c*-axis is shown in Figure 9a. The peaks at ± 2.87 and ± 2.40 MHz are assigned to the $M_S = \pm^1/_2$ manifolds of two of the water protons since these frequencies are outside the range of the powder pattern of $H_{im1,2}$. The assignment of the other lines was done through exchange of the water protons with deuterium by soaking the crystal in D_2O. Henceforth we refer to the D_2O soaked crystal as concanavalin A(D_2O) as opposed to concanavalin A(H_2O). This crystal was mounted like the concanavalin A(H_2O) crystal with its *b*-axis parallel to the tube axis, and ^{1}H and ^{2}H ENDOR spectra were recorded at $\vec{B} \parallel c$ orientation to allow comparison of the ^{1}H spectra of the two crystals. The spectra shown in Figure 9a,b are very similar, except for the collapse of the two resolved signals at ± 1.45 and ± 1.78 MHz and a smaller splitting between the ± 2.87 and ± 2.40 MHz peaks in the spectrum of the concanavalin A(D_2O) crystal due to a small difference in the crystal orientation. The appearance of all the concanavalin A(H_2O) ^{1}H ENDOR lines in the spectrum of concanavalin A(D_2O) indicates that in contrast to the D_2O exchange in solution, which is fast[36] and therefore complete, the water protons in the crystal were only partially exchanged even after 24 h, possibly due to slow diffusion of water in the crystal. The water protons were

(36) Meirovitch, E.; Kalb, A. *J. Biochim. Biophys. Acta* **1973**, 258.

Table 4. Assignment of the ENDOR Frequencies (in MHz) of a Single Crystal of Concanavalin A with the Magnetic Field Along the Crystallographic *c*-Axes

M_S	ν_{im1} (±0.02)	ν_{im2} (±0.02)	ν_{w1} (±0.02)	ν_{w2} (±0.02)	ν_{w3} (±0.02)	ν_{w4} (±0.02)
$-3/2$	−2.7	4.8	−3.0	−4.8		
$-1/2$	−0.85	1.6	−1.0	1.6	−2.6	−2.95
$1/2$	0.85	−1.6	1.0	−1.6	2.6	2.95

assigned by using the ^{2}H Mims ENDOR spectrum of concanavalin A(D_2O) shown in Figure 9c. Three sets of doublets, positioned symmetrically about the Larmor frequency, have been identified as marked on the spectrum. Since the doublets with the largest splitting account for two protons, the three doublets give a total of four protons as expected. Table 4 lists all the ^{1}H ENDOR peaks of the concanavalin A(D_2O) crystal and their assignments. The assignment to the specific M_S manifolds was done as in the frozen solutions. The ^{1}H spectrum recorded at position b (see inset of Figure 9) is shown in Figure 9d. The spectrum is asymmetric and shows contributions mainly from the $M_S = -1/2$ and $-3/2$ manifolds.

Discussion

From the frozen solution measurements it was possible to determine the magnitude and sign of the principal components of the imidazole protons: the values are $A_\perp = -1.72(\pm 0.08)$ MHz, $A_\parallel = 3.54(\pm 0.1)$ MHz. These values yield $a_{iso} = 0.0(\pm 0.1)$, $T_\perp = 1.75(\pm 0.1)$ MHz, and a distance of 3.56 Å between the imidazole proton and the Mn^{2+} ion. The X-ray structure[19] of concanavalin A predicts a Mn−H_{im} distance of 3.5 Å, which is in good agreement with the ENDOR results. Although the two protons are chemically inequivalent, they have the same hyperfine coupling due to the purely dipolar nature of the interaction and their equal distance from the Mn ion. The negligible isotropic hyperfine coupling of these protons supports the assignment of the directly bound nitrogen, rather than the remote nitrogen, as the one responsible for the ESEEM observed at X-band.[21] The orientation of the Mn−H_{im} directions with respect to the *c*-axis can be obtained from the single-crystal ENDOR measurements for the $\vec{B} \parallel c$ orientation by using eq 1. Taking the $H_{im1,2}$ frequencies listed in Table 4 and the value of $T_\perp$ given above angles of 11°(169°) and 84°(96°) were obtained.

The analysis of the ENDOR frequencies of the water protons is more complicated since the four protons were found to be magnetically inequivalent. Although four different values of $A_\parallel$ and $A_\perp$ were determined from the frozen solution measurements, the specific pairs that belong to the individual protons cannot be determined from the available data and require complete single-crystal measurements. Here we consider all 16 possible combinations, as listed in Table 5. For each combination, a_{iso}, $T_\perp$, and *r* were calculated (Table 5) and all distances were found to be between 2.67 and 3.24 Å. Similar ENDOR measurements on $Mn(H_2O)_6^{2+}$ in a frozen solution gave $A_\parallel = 7.64(\pm 0.1)$ MHz and $A_\perp = -2.77(\pm 0.08)$ MHz, yielding $a_{iso} = 0.7(\pm 0.08)$ MHz, $T_\perp = 3.48(\pm 0.1)$ MHz, and $r = 2.8(\pm 0.04)$ Å, in agreement with earlier X-band ENDOR results.[29] If we assume that the mechanism leading to the isotropic hyperfine coupling of the water protons is the same as in the hexa-aquo complex, then all the combinations that generate negative a_{iso} values can be eliminated. This leaves Mn−H distances of 2.67(±0.04), 2.76(±0.04), 2.99(±0.04), and 3.24(±0.04) Å. Complete single-crystal measurements can provide unambiguous assignment of the $A_\parallel$, $A_\perp$ pairs. Considering the low symmetry of the Mn^{2+} site, the different chemical environments of the four water molecules and their possible involvement in hydrogen bonding, it is not surprising that they span over a range of distances. In a recent 2.4 Å resolution neutron Laue diffraction study of a single crystal of concanavalin A at 298 K,[37] nuclear density corresponding to the four deuterium atoms of the two Mn-bound water molecules was detected and the individual Mn−D distances were determined to be 2.63, 2.77, 2.87, and 3.08 Å, in good agreement with the values found in the present ENDOR study at 4.4 K.

Table 5. All Possible Combinations of $A_\parallel$ and $A_\perp$ for the Water Protons and the Corresponding a_{iso} (MHz), $T_\perp$, and *r* Values

$A_\perp$ (±0.1), MHz	$A_\parallel$ (±0.08), MHz	a_{iso} (±0.08), MHz	$T_\perp$ (±0.1), MHz	*r* (±0.04), Å
−2.12	4.86	0.21	2.37	3.24
−2.12	7.54	1.1	3.22	2.90
−2.12	6.0	0.59	2.70	3.08
−2.12	8.33	1.37	3.48	2.82
−2.88	4.86	−0.3	2.51	3.12
−2.88	7.54	0.59	3.47	2.83
−2.88	6.0	0.08	2.96	2.99
−2.88	8.33	0.86	3.74	2.76
−3.72	4.86	−0.86	2.86	3.02
−3.72	7.54	0.03	3.75	2.76
−3.72	6.0	−0.48	3.24	2.91
−3.72	8.33	0.29	4.01	2.67
−4.13	4.86	−1.13	3.0	2.97
−4.13	7.54	−0.24	3.89	2.73
−4.13	6.0	−0.75	3.37	2.86
−4.13	8.33	0.03	4.15	2.67

The experiments carried out on a frozen solution are useful for assignment of the signals in single crystal measurements as they provide the limits of the hyperfine splitting of the various protons. Detailed single crystal measurements designed to determine the full hyperfine tensors of the water and imidazole protons are currently under way.

Conclusions

W-band pulsed ENDOR experiments were performed on frozen solutions of the protein concanavalin A. Selection of different EPR transitions together with exchange with D_2O allowed the assignment of the imidazole and water protons and the determination of the magnitude and sign of the principal components of the hyperfine interaction. The two imidazole protons are magnetically equivalent, situated 3.56 Å from the Mn^{2+} in the transition-metal-binding site, S1, and their hyperfine coupling is purely dipolar. The protons of the two water ligands are all inequivalent, characterized by four distinct values of $A_\parallel$ and $A_\perp$. The possible combinations of these values yield Mn−H distances in the range 2.67−3.24 Å.

Single-crystal measurements show that the individual crystallographic sites of Mn^{2+} are well resolved in the FS-ED EPR spectra at W-band, facilitating single-crystal ENDOR measurements where the same strategy for signal assignment used for the frozen solution is applied.

Acknowledgments. This research was supported by the DFG Schwerpunkt program "High field EPR in Physics, Chemistry and Biology", the Israel Science Foundation administered by the Israel Academy of Sciences and Humanities, and the UK-Israel Science and Technology Research Fund. We thank the authors of ref 37 for making it available to us before publication.

JA993395Z

(37) Habash, J.; Raftery, J.; Nuttall, R.; Price, H. J.; Wilkinson, C.; Kalb (Gilboa), A. J.; Helliwell, J. R. *Acta Crystallogr.* **2000**, *D56* (in press).